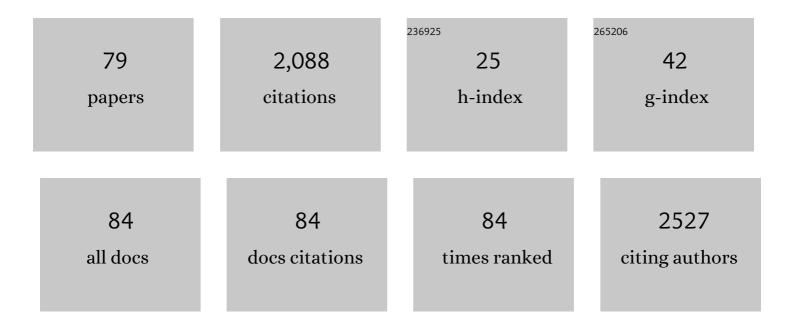
List of Publications by Year in descending order

Source: https://exaly.com/author-pdf/5849465/publications.pdf Version: 2024-02-01



#	Article	IF	CITATIONS
1	Overhauser enhanced magnetic resonance imaging for tumor oximetry: Coregistration of tumor anatomy and tissue oxygen concentration. Proceedings of the National Academy of Sciences of the United States of America, 2002, 99, 2216-2221.	7.1	284
2	Nitric Oxide Protects against the Cytotoxic Effects of Reactive Oxygen Species. Annals of the New York Academy of Sciences, 1994, 738, 265-278.	3.8	89
3	Targeting ABL1-Mediated Oxidative Stress Adaptation in Fumarate Hydratase-Deficient Cancer. Cancer Cell, 2014, 26, 840-850.	16.8	87
4	Targeting Glycolysis through Inhibition of Lactate Dehydrogenase Impairs Tumor Growth in Preclinical Models of Ewing Sarcoma. Cancer Research, 2019, 79, 5060-5073.	0.9	86
5	In vivo imaging of a stable paramagnetic probe by pulsed-radiofrequency electron paramagnetic resonance spectroscopy. Magnetic Resonance in Medicine, 1997, 38, 409-414.	3.0	84
6	Dynamic Imaging of LDH Inhibition in Tumors Reveals Rapid InÂVivo Metabolic Rewiring and Vulnerability to Combination Therapy. Cell Reports, 2020, 30, 1798-1810.e4.	6.4	73
7	Radiation, Radicals, and Images. Annals of the New York Academy of Sciences, 2000, 899, 28-43.	3.8	62
8	Electron Paramagnetic Resonance Imaging of Tumor pO ₂ . Radiation Research, 2012, 177, 376-386.	1.5	61
9	Magnetic Resonance Imaging of the Tumor Microenvironment in Radiotherapy: Perfusion, Hypoxia, and Metabolism. Seminars in Radiation Oncology, 2014, 24, 210-217.	2.2	61
10	Three-dimensional whole body imaging of spin probes in mice by time-domain radiofrequency electron paramagnetic resonance. Magnetic Resonance in Medicine, 2000, 43, 375-382.	3.0	58
11	Dynamic Imaging of Glucose and Lactate Metabolism by 13C-MRS without Hyperpolarization. Scientific Reports, 2019, 9, 3410.	3.3	56
12	A broadband pulsed radio frequency electron paramagnetic resonance spectrometer for biological applications. Review of Scientific Instruments, 1998, 69, 1869-1876.	1.3	55
13	13C-MR Spectroscopic Imaging with Hyperpolarized [1-13C]pyruvate Detects Early Response to Radiotherapy in SCC Tumors and HT-29 Tumors. Clinical Cancer Research, 2015, 21, 5073-5081.	7.0	54
14	Evaluation of oxygen dependence on in vitro and in vivo cytotoxicity of photoimmunotherapy using IR-700–antibody conjugates. Free Radical Biology and Medicine, 2015, 85, 24-32.	2.9	45
15	Gadolinium-labeled dendrimers as biometric nanoprobes to detect vascular permeability. Journal of Materials Chemistry, 2003, 13, 1523.	6.7	44
16	Metabolic and Physiologic Imaging Biomarkers of the Tumor Microenvironment Predict Treatment Outcome with Radiation or a Hypoxia-Activated Prodrug in Mice. Cancer Research, 2018, 78, 3783-3792.	0.9	42
17	<i>In Vivo</i> Imaging of Tumor Physiological, Metabolic, and Redox Changes in Response to the Anti-Angiogenic Agent Sunitinib: Longitudinal Assessment to Identify Transient Vascular Renormalization. Antioxidants and Redox Signaling, 2014, 21, 1145-1155.	5.4	41
18	Hyperpolarized [1-13C]-Pyruvate Magnetic Resonance Spectroscopic Imaging of Prostate Cancer <i>In Vivo</i> Predicts Efficacy of Targeting the Warburg Effect. Clinical Cancer Research, 2018, 24, 3137-3148.	7.0	36

#	Article	IF	CITATIONS
19	Pyruvate Induces Transient Tumor Hypoxia by Enhancing Mitochondrial Oxygen Consumption and Potentiates the Anti-Tumor Effect of a Hypoxia-Activated Prodrug TH-302. PLoS ONE, 2014, 9, e107995.	2.5	35
20	Pulsed Electron Paramagnetic Resonance Imaging: Applications in the Studies of Tumor Physiology. Antioxidants and Redox Signaling, 2018, 28, 1378-1393.	5.4	33
21	Protection Against Oxidative Stress by Nitroxides. Experimental Biology and Medicine, 2001, 226, 620-621.	2.4	30
22	<i>In Vivo</i> Application of Proton-Electron Double-Resonance Imaging. Antioxidants and Redox Signaling, 2018, 28, 1345-1364.	5.4	30
23	Glycolytic metabolism of pathogenic T cells enables early detection of GVHD by 13C-MRI. Blood, 2021, 137, 126-137.	1.4	29
24	Nitroxides as antioxidants: Tempol protects against EO9 cytotoxicity. Molecular and Cellular Biochemistry, 2002, 234/235, 327-333.	3.1	27
25	Radiotherapy Synergizes with the Hypoxia-Activated Prodrug Evofosfamide: In Vitro and In Vivo Studies. Antioxidants and Redox Signaling, 2018, 28, 131-140.	5.4	27
26	Tensor image enhancement and optimal multichannel receiver combination analyses for human hyperpolarized ¹³ C MRSI. Magnetic Resonance in Medicine, 2020, 84, 3351-3365.	3.0	27
27	Hypoxia-Activated Prodrug Evofosfamide Treatment in Pancreatic Ductal Adenocarcinoma Xenografts Alters the Tumor Redox Status to Potentiate Radiotherapy. Antioxidants and Redox Signaling, 2021, 35, 904-915.	5.4	26
28	Oral administration of the nitroxide radical TEMPOL exhibits immunomodulatory and therapeutic properties in multiple sclerosis models. Brain, Behavior, and Immunity, 2017, 62, 332-343.	4.1	24
29	Molecular Imaging of the Tumor Microenvironment Reveals the Relationship between Tumor Oxygenation, Glucose Uptake, and Glycolysis in Pancreatic Ductal Adenocarcinoma. Cancer Research, 2020, 80, 2087-2093.	0.9	24
30	Suberoylanilide hydroxamic acid radiosensitizes tumor hypoxic cells in vitro through the oxidation of nitroxyl to nitric oxide. Free Radical Biology and Medicine, 2014, 73, 291-298.	2.9	23
31	Highâ€speed digitizer/averager dataâ€acquisition system for Fourier transform electron paramagnetic resonance spectroscopy. Review of Scientific Instruments, 1994, 65, 2500-2504.	1.3	19
32	Nitroxides as Radiation Protectors. Military Medicine, 2002, 167, 49-50.	0.8	19
33	Imaging of glucose metabolism by 13C-MRI distinguishes pancreatic cancer subtypes in mice. ELife, 2019, 8, .	6.0	19
34	Magnetic resonance imaging of tumor oxygenation and metabolic profile. Acta Oncológica, 2013, 52, 1248-1256.	1.8	17
35	A radical containing injectable in-situ-oleogel and emulgel for prolonged in-vivo oxygen measurements with CW EPR. Free Radical Biology and Medicine, 2019, 130, 120-127.	2.9	17
36	Multimodal Functional Imaging for Cancer/Tumor Microenvironments Based on MRI, EPRI, and PET. Molecules, 2021, 26, 1614.	3.8	17

#	Article	IF	CITATIONS
37	Quantitative imaging of pO ₂ in orthotopic murine gliomas: hypoxia correlates with resistance to radiation. Free Radical Research, 2017, 51, 861-871.	3.3	16
38	Molecular imaging of tumor photoimmunotherapy: Evidence of photosensitized tumor necrosis and hemodynamic changes. Free Radical Biology and Medicine, 2018, 116, 1-10.	2.9	16
39	A Multimodal Molecular Imaging Study Evaluates Pharmacological Alteration of the Tumor Microenvironment to Improve Radiation Response. Cancer Research, 2018, 78, 6828-6837.	0.9	16
40	Maximum Entropy Reconstruction Methods in Electron Paramagnetic Resonance Imaging. Annals of Operations Research, 2003, 119, 101-118.	4.1	15
41	Multimodal Molecular Imaging Detects Early Responses to Immune Checkpoint Blockade. Cancer Research, 2021, 81, 3693-3705.	0.9	15
42	Effect of amifostine, a radiation-protecting drug, on oxygen concentration in tissue measured by EPR oximetry and imaging. Journal of Clinical Biochemistry and Nutrition, 2017, 60, 151-155.	1.4	14
43	Comparative studies with EPR and MRI on the <i>in vivo</i> tissue redox status estimation using redox-sensitive nitroxyl probes: influence of the choice of the region of interest. Free Radical Research, 2018, 52, 248-255.	3.3	14
44	Three-dimensional alginate hydrogels for radiobiological and metabolic studies of cancer cells. Colloids and Surfaces B: Biointerfaces, 2018, 171, 197-204.	5.0	14
45	Multimodality Imaging Identifies Distinct Metabolic Profiles In Vitro and In Vivo. Neoplasia, 2016, 18, 742-752.	5.3	13
46	Radiation-Induced Senescence Reprograms Secretory and Metabolic Pathways in Colon Cancer HCT-116 Cells. International Journal of Molecular Sciences, 2021, 22, 4835.	4.1	13
47	Hypoxia Imaging As a Guide for Hypoxia-Modulated and Hypoxia-Activated Therapy. Antioxidants and Redox Signaling, 2022, 36, 144-159.	5.4	13
48	<scp>EPR</scp> â€based oximetric imaging: a combination of single pointâ€based spatial encoding and <scp>T</scp> ₁ weighting. Magnetic Resonance in Medicine, 2018, 80, 2275-2287.	3.0	12
49	Multi-modality imaging to assess metabolic response to dichloroacetate treatment in tumor models. Oncotarget, 2016, 7, 81741-81749.	1.8	10
50	Structure-guided design enables development of a hyperpolarized molecular probe for the detection of aminopeptidase N activity in vivo. Science Advances, 2022, 8, eabj2667.	10.3	10
51	Identification of high-risk drugs related to chemotherapy-induced peripheral neuropathyÂin Cancer Therapy Evaluation Program–sponsored phase I trials. European Journal of Cancer, 2019, 115, 111-119.	2.8	9
52	Synthesis and evaluation of 13C-labeled 5-5-dimethyl-1-pyrroline-N-oxide aimed at in vivo detection of reactive oxygen species using hyperpolarized 13C-MRI. Free Radical Biology and Medicine, 2019, 131, 18-26.	2.9	9
53	Development of Functional Electron Paramagnetic Resonance Imaging. Breast Disease, 1998, 10, 209-220.	0.8	8
54	Co-imaging of the tumor oxygenation and metabolism using electron paramagnetic resonance imaging and 13-C hyperpolarized magnetic resonance imaging before and after irradiation. Oncotarget, 2018, 9, 25089-25100.	1.8	8

#	Article	IF	CITATIONS
55	Cancer Incidence in C3H Mice Protected from Lethal Total-Body Radiation after Amifostine. Radiation Research, 2018, 189, 490-496.	1.5	7
56	Effects of oxygen challenging to tissue redox and pO2 status. Free Radical Biology and Medicine, 2019, 130, 343-347.	2.9	7
57	The antioxidant tempol transforms gut microbiome to resist obesity in female C3H mice fed a high fat diet. Free Radical Biology and Medicine, 2022, 178, 380-390.	2.9	7
58	Direct and indirect assessment of cancer metabolism explored by MRI. NMR in Biomedicine, 2019, 32, e3966.	2.8	6
59	Trehalose as an alternative to glycerol as a glassing agent for in vivo DNP MRI. Magnetic Resonance in Medicine, 2021, 85, 42-48.	3.0	6
60	Detection of metabolic change in glioblastoma cells after radiotherapy using hyperpolarized ¹³ Câ€MRI. NMR in Biomedicine, 2021, 34, e4514.	2.8	6
61	Real-Time insight into in vivo redox status utilizing hyperpolarized [1-13C] N-acetyl cysteine. Scientific Reports, 2021, 11, 12155.	3.3	6
62	Synthesis of [1â€ ¹³ Câ€5â€ ¹² C]â€alphaâ€ketoglutarate enables noninvasive detection 2â€hydroxyglutarate. NMR in Biomedicine, 2021, 34, e4588.	n of 2.8	6
63	Simple Esterification of [1- ¹³ C]-Alpha-Ketoglutarate Enhances Membrane Permeability and Allows for Noninvasive Tracing of Glutamate and Glutamine Production. ACS Chemical Biology, 2021, 16, 2144-2150.	3.4	6
64	PEGPH20, a PEGylated human hyaluronidase, induces radiosensitization by reoxygenation in pancreatic cancer xenografts. A molecular imaging study. Neoplasia, 2022, 30, 100793.	5.3	6
65	Redox Mapping of Biological Samples Using EPR Imaging. Israel Journal of Chemistry, 2008, 48, 27-31.	2.3	5
66	Effect of body temperature on the pharmacokinetics of a triarylmethylâ€ŧype paramagnetic contrast agent used in EPR oximetry. Magnetic Resonance in Medicine, 2018, 79, 1212-1218.	3.0	4
67	An efficient synthesis of 3-(N-piperidinemethyl)-2,2,5,5-tetramethyl-1-oxy-3-pyrroline, a promising radioprotector for cancer radiotherapy. Tetrahedron Letters, 2014, 55, 5570-5571.	1.4	3
68	Passive Decoupling Due to Low Q-Factors of Four-Channel Coils in 300-MHz Pulsed EPR Imaging. Applied Magnetic Resonance, 2015, 46, 671-683.	1.2	3
69	Imaging Metabolic Processes to Predict Radiation Responses. Seminars in Radiation Oncology, 2019, 29, 81-89.	2.2	3
70	Towards reduction of SAR in scaling up in vivo pulsed EPR imaging to larger objects. Journal of Magnetic Resonance, 2019, 299, 42-48.	2.1	3
71	A Feature Identification System for Electron Magnetic Resonance Tomography: Fusion of Principal Components Transform, Color Quantization and Boundary Information. Journal of Mathematical Imaging and Vision, 2008, 30, 284-297.	1.3	2
72	Electron paramagnetic resonance imaging. Resonance, 2016, 21, 717-740.	0.3	2

#	Article	IF	CITATIONS
73	Wireless implantable coil with parametric amplification for in vivo electron paramagnetic resonance oximetric applications. Magnetic Resonance in Medicine, 2018, 80, 2288-2298.	3.0	2
74	Special Issues of AMR on the Occasion of the 85th Birthday of Harold M. Swartz (HMS): Overview of Part 2 Articles and HMS' Citations on Magnetic Resonance. Applied Magnetic Resonance, 2022, 53, 1-45.	1.2	2
75	EPR oxygen imaging and hyperpolarized 13 C MRI of pyruvate metabolism as noninvasive biomarkers of tumor treatment response to a glycolysis inhibitor 3-bromopyruvate. Magnetic Resonance in Medicine, 2013, 69, spcone-spcone.	3.0	1
76	Electron Paramagnetic Resonance imaging. Resonance, 2016, 21, 597-619.	0.3	1
77	The Development of Time-Domain In Vivo EPR Imaging at NCI. Applied Magnetic Resonance, 2021, 52, 1291-1309.	1.2	1
78	Special Issues of AMR on the Occasion of the 85th Birthday of Harold M. Swartz. Applied Magnetic Resonance, 0, , 1.	1.2	0
79	Abstract 5974: Multimodal molecular imaging detects early reoxygenation induced by hyaluronan depletion in pancreatic cancer model mouse. Cancer Research, 2022, 82, 5974-5974.	0.9	0